IEEE Open Journal of
Power Electronics

Received 12 January 2021; revised 15 February 2021; accepted 17 February 2021. Date of publication 22 February 2021; date of current version 9 March 2021. The review of this article was arranged by Associate Editor Dr. X. Yao.

Digital Object Identifier 10.1109/OJPEL.2021.3060874

iGSE-C_x – a New Normalized Steinmetz Model for Class II Multilayer Ceramic Capacitors

DAVID MENZI (Student Member, IEEE), MORRIS HELLER (Student Member, IEEE), AND JOHANN W. KOLAR (Fellow, IEEE)

Power Electronic Systems Laboratory (PES), ETH Zurich, 8092 Zürich, Switzerland

CORRESPONDING AUTHOR: DAVID MENZI (e-mail: menzi@lem.ee.ethz.ch)

ABSTRACT Ferroelectric Class II ceramic capacitors allow for highly compact converter realizations, but are showing relatively high losses for large-signal excitations which must be taken into account in the system dimensioning. Recent literature introduced the iGSE-C_Q, a Steinmetz model based on the macroscopic capacitor Q-U hysteresis, allowing to accurately predict the losses of X7R capacitors. However, the model is specific for each single device, i.e., is insufficient to characterize losses in devices of the same series and manufacturer, which are employing the same dielectric material but with different voltage rating or nominal capacitance value. In this publication, based on basic physical properties we propose a new Steinmetz model, the iGSE-C_X based on the relative dielectric material D-E hysteresis, which is applicable to all devices of a capacitor series. The iGSE-C_X loss modeling technique is demonstrated for the TDK X7R, the TDK X7T, as well as the Knowles Syfer X7R series. Finally, the iGSE-C_X is employed to estimate the large-signal losses of the capacitors of a three-phase inverter and shown to offer sufficient accuracy for a first power circuit design.

INDEX TERMS AC-DC power converters, DC-AC power converters, iGSE, iGSE-C, inverters, loss modeling, MLCC, multilayer ceramic capacitor, power capacitors, rectifiers, steinmetz equation.

NOMENCLATURE

P, W	MLCC large-signal excitation losses, dissipated energy per cycle
U, Q, f, T	Excitation voltage, charge, frequency and period
k_Q, α, β	Steinmetz parameters[1] (charge-based iGSE-C_Q)
C, C_Q	Differential and charge equivalent capacitance
$\varepsilon, \overline{\varepsilon}$	Differential and average dielectric constant
V, A, t	MLCC internal dimensions: dielectric volume, active area and layer thickness
E, D, ρ	Electric field, displacement field and dielectric loss density
k_D, α, β	Steinmetz param.[1] (D-field based iGSE-C_D)
E_{max}	Maximum admissible E-field
C_0, U_R, δ_C	Datasheet parameters: nominal capacitance, rated voltage and capacitance tolerance
E_x, D_x, P_x	Relative electric field, displacement field and losses
k_x, α, β	Steinmetz param.[1] (D_x-field based iGSE-C_X)
$\epsilon_{Dx}, \epsilon_P$	Modeling error for relative displacement field and device losses

[1]The Steinmetz parameters α and β are identical for the considered iGSE-C_Q, iGSE-C_D and iGSE-C_X loss models.

I. INTRODUCTION

Multilayer Ceramic Capacitor (MLCC) with ferroelectric Class II dielectrics show a large relative permittivity and high energy densities [1], [2] and hence are the preferred capacitor technology for ultra-compact converter systems [3], [4]. Fig. 1 shows as an example the main power circuit of a motor drive system powered from the three-phase mains, where MLCCs can be applied in ① the grid-side filter to suppress conducted Electromagnetic Interference (EMI) emissions towards the mains, ② as DC-link capacitor, or also in ③ a sinewave filter reducing the dv/dt-stress on the motor winding insulation and the high-frequency motor losses [5], [6]. Note that, while the grid-filter voltages ① are (almost perfectly) sinusoidal and constant in magnitude, the motor sine-filter voltages ③ vary in frequency and magnitude based on the motor speed

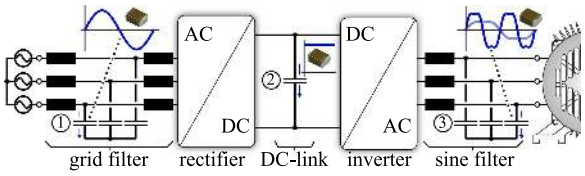

FIGURE 1. Main power circuit of a motor drive system powered from the three-phase mains, where possible MLCC voltage waveforms are highlighted.

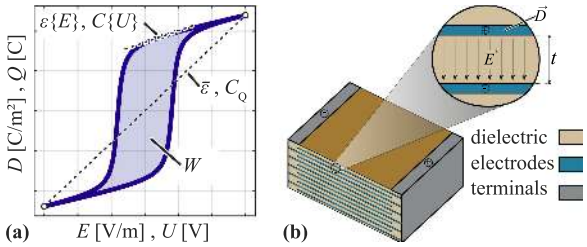

FIGURE 2. (a) Ferroelectric $Q-U$ (or $D-E$) hysteresis loop, with differential capacitance $C\{U\}$ (or differential permittivity $\varepsilon\{E\}$) highlighted separately from the average large-signal charge equivalent capacitance $C_Q = Q_{pk}/U_{pk}$ (or average permittivity $\bar{\varepsilon} = D_{pk}/E_{pk}$) [13]. Note that W represents the dissipated energy during one fundamental period T. (b) Illustration of the internal structure of an MLCC formed by several geometrically interleaved electrodes and dielectric layers.

and may also contain frequency components at multiples of the fundamental frequency (e.g., for third harmonic injection modulation [7]) to enable a maximum utilization of the DC-link voltage for AC voltage formation. MLCCs further find application in active power pulsation buffers of ultra-compact single-phase rectifiers [8]–[10], where the MLCCs are subject to a large power-dependent voltage swing at twice the mains frequency.

It is important to highlight, that the ultra-high dielectric constant of Class II MLCCs comes at the cost of a non-linear voltage-dependent capacitance value [11]–[14]. Moreover, high low-frequency large-signal excitation dissipation factors and losses (causing substantial device heating) were reported, where the losses depend on the AC voltage amplitude, frequency and shape (third harmonic injection), as well as DC-bias and temperature [8], [15], [16].

According to [17] small-signal measurements are fundamentally insufficient to characterize Class II MLCCs, and a large-signal dissipation factor elevated by a factor of 10 (!) compared to small-signal measurements was found in [16].

Therefore, in order to accurately predict the losses P of MLCCs under various large-signal excitation conditions (cf. Fig. 1), the peak charge excitation-based *improved Generalized Steinmetz Equation for Ceramic Capacitors* (iGSE-C_Q) was proposed in [16],

$$P = k_Q \cdot f^{\alpha} \cdot Q_{pk}^{\beta}, \tag{1}$$

with the AC frequency f and the peak charge Q_{pk}, while k_Q, α, and β are device-specific parameters determined for large-signal excitation. The iGSE-C_Q was verified for a 1kV X7R MLCC (2220Y1K00474KETWS2), where $\alpha = 1$ was found, such that (1) also accurately predicts losses for non-sinusoidal excitation voltage waveforms with minor loops. Further, the obtained iGSE-C_Q parameters were found to be DC-bias *invariant*, i.e only the resulting capacitance value is impacted by a DC-bias voltage, while the charge-loss relationship characterized by β in (1) remains unaffected.

However, the obtained iGSE-C_Q parameters of (1) are limited to the evaluated individual device, i.e., are not even applicable for devices with the same dielectric material but different capacitance value or voltage rating. This represents a major limitation of the model and a clear difference to the Steinmetz loss modeling of magnetic materials.

To overcome this shortcoming, in Section II we derive a new normalized Steinmetz loss model based on basic capacitor voltage and capacitance scaling laws that describes the losses of a complete MLCC series (i.e., a manufacturer device series with same relative geometries and the same dielectric material, but with different rated voltages and capacitance values) with a single set of Steinmetz parameters. The new loss model is verified in Section III by means of measured losses obtained by an automated Sawyer-Tower [16] measurement setup, where the losses of the TDK X7R, the TDK X7T and the Knowles Syfer X7R MLCC series are recorded for devices with various rated voltage and nominal capacitance values. A design example using the iGSE-C_X is provided in Section IV, and finally, in Section V the main properties of the proposed iGSE-C_X and the findings of the experimental verification are summarized.

II. STEINMETZ PARAMETER NORMALIZATION

The limitation of the proposed iGSE-C_Q becomes obvious by considering two identical (parallel connected) MLCC devices exited with the same voltage resulting in twice the peak charge Q_{pk} compared to a single MLCC, while also the sum of the losses doubles. However, the iGSE-C_Q (1) predicts 2^{β} times the losses of a single device due to the charge doubling, such that for any $\beta \neq 1$ the losses predicted by iGSE-C_Q for this example are wrong.

This results as the iGSE-C_Q considers the macroscopic $Q-U$ hysteresis, where the losses scale with the hysteresis loop area, instead of the actual physical $D-E$ hysteresis, where the dielectric loss *density* ρ scales with the loop area (cf. Fig. 2(a) [16], [18]. Note that for a given voltage excitation U and related charge Q, the E-field excitation and resulting D-field (as well as the differential $\varepsilon\{E\}$ and average dielectric constant $\bar{\varepsilon}$) are directly defined by the device geometry,

$$\begin{aligned} E &= U/t \\ D &= Q/A \\ V &= A \cdot t, \end{aligned} \tag{2}$$

as illustrated in Fig. 2(b) and with A the active area (i.e., the electrode overlap area multiplied by the number of dielectric layers), t the layer thickness and V the dielectric volume.

Accordingly, the dielectric losses P can also be described based on the peak displacement field D_{pk} and the dielectric volume V as

$$P = \rho V = k_{\mathrm{D}} \cdot f^{\alpha} \cdot D_{\mathrm{pk}}^{\beta} \cdot V, \tag{3}$$

which is further referred to as iGSE-C_{D}. In the aforementioned example of paralleling two identical MLCCs, the dielectric volume is doubled, while the D-field and E-field excitation (and hence also the dielectric loss density ρ) remain unaffected, such that the calculated losses according to (3) correctly double. It is important to highlight, that parameters α and β are identical in (1) and (3), while the coefficient k_{D} is given by

$$k_{\mathrm{D}} = \frac{k_{\mathrm{Q}}}{V}\left(\frac{Q_{\mathrm{pk}}}{D_{\mathrm{pk}}}\right)^{\beta} \overset{(2)}{=} \frac{k_{\mathrm{Q}}}{V} A^{\beta}. \tag{4}$$

Hence, for a characterized device with fitted iGSE-C_{Q} parameters and known internal structure (i.e., A and t), the *material-specific* coefficient k_{D} can be calculated with (4).

However, the internal structure of MLCCs is typically not published by device manufacturers, and therefore in the following we employ the concept of the iGSE-C_{D} and basic physical capacitor properties to derive a new loss model which generalizes *device-specific* into *material-specific* properties and accordingly can be applied to all devices of an MLCC series, while only the device rated voltage U_{R} and nominal capacitance C_0 (i.e., information known from the datasheet) is required.

As MLCCs show large horizontal dimensions compared to the dielectric layer thickness t (measured in vertical direction), the capacitance value C can be approximated with

$$C = \frac{\varepsilon\{E\}A}{t} \overset{(2)}{=} \frac{\varepsilon\{U/t\}A}{t}, \tag{5}$$

where $\varepsilon\{E\}$ is the E-field dependent permittivity specific to the employed dielectric material ($C_0 = C\{U = 0V\}$). Note that (2) and (5) yield an economic incentive to minimize the layer thickness t, in order to maximize the volumetric nominal capacitance density. However, for a given rated voltage U_{R}, a lower bound for the layer thickness t is given by the maximum admissible electric field strength of the dielectric material $E_{\max}$ with $t \geq U_{\mathrm{R}}/E_{\max}$.

In the following we therefore assume the dielectric layer thickness t to scale linearly with the device rated voltage U_{R} (which holds according to [19] up to $U_{\mathrm{R}} = 1kV$), and hence the relations between the device geometrical dimensions (i.e., layer thickness t, total area A, dielectric volume V) and the nominal device values (i.e., nominal capacitance C_0 and rated voltage U_{R}):

$$\begin{aligned} t &\propto U_{\mathrm{R}} \\ &\overset{(5)}{\rightarrow} A \propto U_{\mathrm{R}} C_0 \\ &\overset{(2)}{\rightarrow} V \propto U_{\mathrm{R}}^2 C_0. \end{aligned} \tag{6}$$

Combining (4) with (6), a linear scaling of k_{D} with the device-specific k_{Q} (depending on device rated voltage U_{R} and nominal capacitance C_0) results to

$$k_{\mathrm{D}} \propto k_{\mathrm{Q}} \cdot C_0^{\beta-1} \cdot U_{\mathrm{R}}^{\beta-2} \equiv k_{\mathrm{x}}, \tag{7}$$

where k_{x} scales linearly with k_{D}, hence represents material-specific properties, while k_{x} can be calculated from k_{Q} with the nominal device parameters U_{R} and C_0 only.

Similarly, according to (2) and (6) the E-field scales linearly with the excitation voltage U and according to (2) and (5) the D-field scales linearly with the device charge Q, resulting in

$$\begin{aligned} E\{U\} &\propto \frac{U}{U_{\mathrm{R}}} \equiv E_{\mathrm{x}}\{U\} \\ D\{E\} &\propto \frac{Q\{E_{\mathrm{x}}\}}{U_{\mathrm{R}} C_0} \equiv D_{\mathrm{x}}\{E_{\mathrm{x}}\}. \end{aligned} \tag{8}$$

There, the relative electric field excitation E_{x} scales linearly with E, and the relative electric displacement field D_{x} scales linearly with D, hence both represent material-specific properties, while only the nominal device parameters U_{R} and C_0 are required to obtain the unitless quantities $D_{\mathrm{x}}\{E_{\mathrm{x}}\}$ and E_{x} for a measured charge $Q\{U\}$ and voltage U. With (7) and (8), the iGSE-C_{Q} (1) can now be generalized

$$\begin{aligned} P &= \underbrace{k_{\mathrm{x}} C_0^{1-\beta} U_{\mathrm{R}}^{2-\beta}}_{k_{\mathrm{Q}}} \cdot f^{\alpha} \cdot \underbrace{(D_{\mathrm{x}} U_{\mathrm{R}} C_0)^{\beta}}_{Q\mathrm{pk}^{\beta}} \\ &= \boxed{k_{\mathrm{x}} \cdot f^{\alpha} \cdot D_{\mathrm{x}}^{\beta} \cdot U_{\mathrm{R}}^2 C_0}, \end{aligned} \tag{9}$$

which only depends on the relative electric displacement field D_{x} and is further referred to as the iGSE-C_{X}. Finally, relative MLCC losses P_{x} can be defined from (9)

$$P_{\mathrm{x}} = \frac{P}{U_{\mathrm{R}}^2 C_0 f} \overset{\alpha=1}{=} k_{\mathrm{x}} D_{\mathrm{x}}^{\beta}, \tag{10}$$

which depend (for $\alpha = 1$, as is given for the Class II MLCCs considered here [16]) only on the relative displacement field excitation D_{x} and the iGSE-C_{X} parameter k_{x}. Hence, as will be verified in the following, the losses of a complete MLCC series can be calculated with the iGSE-C_{X} (9) and based on a single curve $D_{\mathrm{x}}\{U/U_{\mathrm{R}}\}$, and the parameters k_{x}, α and β.

III. EXPERIMENTAL VERIFICATION

The devices of the MLCC series listed in Table I are evaluated using an automated MLCC loss measurement setup based on the Sawyer-Tower circuit [16], where AC voltages up to $270V_{\mathrm{rms}}$ (limit of the employed AC source), are applied while the peak charge Q_{pk} and the losses P are recorded. As $\alpha = 1$ was found in [16] for frequencies up to 500 Hz, the measurements are conducted for a single frequency of 100 Hz. Device details and the extracted iGSE-C_{Q} parameters are listed in the Appendix A.

The scatter points in Fig. 3(a) show the obtained relative losses P_{x} over the relative displacement field D_{x}, where D_{x} is derived from the measured charge Q according to

TABLE I Considered MLCC Series (Device Details are Provided in Appendix A)

Manuf.	Diel.	#	U_R	C_0	k_x	β	$D_x\{E_x\}$	ϵ_{Dx}	ϵ_P
TDK	X7R [21]	7	250 V..630 V	0.1 uF..1 µF	0.23	2.29	$1.22E_x - 0.60E_x^2$	6 %	+17 % / -15 %
TDK	X7T [21]	15	250 V..630 V	0.1 uF..2.2 µF	0.07	2.19	$1.02E_x - 0.41E_x^2$	13 %	+43 % / -26 %
Knowles	X7R [22]	16	200 V..1 kV	0.1 nF..2.2 µF	0.26	2.28	$1.14E_x - 0.59E_x^2$	22 %	+51 % / -30 %

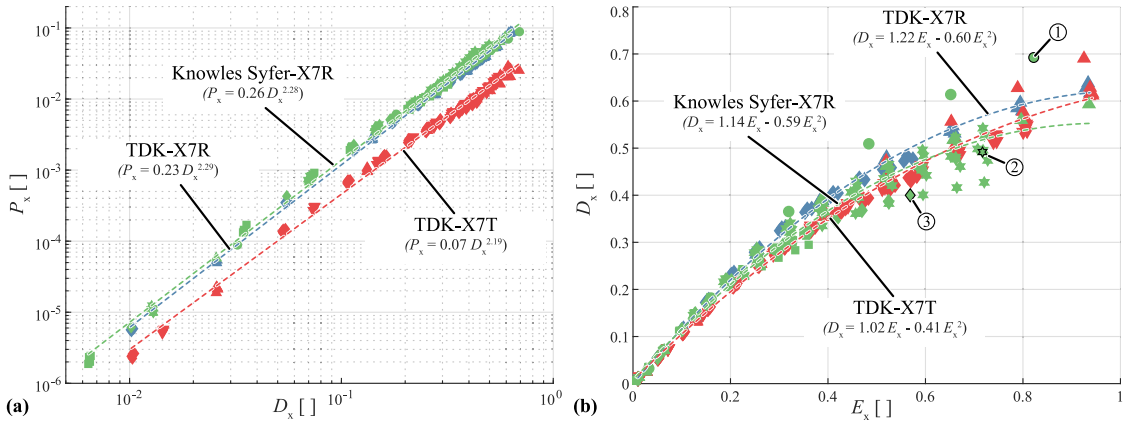

FIGURE 3. (a) Measured relative losses P_x (cf. (10)) over relative displacement field D_x (cf. (8)), and (b) relative displacement field D_x over relative electric field excitation E_x (cf. (8)) for the MLCC series listed in Table I (device details are provided in Appendix A).

(8) and employing the datasheet rated voltage U_R and measured C_0 for a sinusoidal small-signal AC excitation voltage of $5V_{rms}$. The logarithmic plot reveals a power law relationship of P_x and D_x specific to each MLCC series, confirming hence the approach of the iGSE-C_X according to (9), while the dashed lines in Fig. 3(a) represent the obtained iGSE-C_X-Steinmetz-fit with parameters k_x, β (and $\alpha = 1$). Please note, that in contrast to magnetic components with Steinmetz parameters varying with the AC magnetic flux density peak value B_{pk} (i.e., a Steinmetz parameter set is only valid for a limited range of B_{pk} [20]), here, the results in Fig. 3(a) reveal that the relative losses P_x can be described with reasonable accuracy with a single set of Steinmetz parameters for a range in relative displacement field D_x of two orders of magnitude. Further, the results in Fig. 3(a) identify an improved loss performance (i.e., lower iGSE-C_X parameters k_x and β) of the X7T dielectric compared to the X7R dielectrics. Here it is important to highlight, that the improved loss performance of X7T MLCCs comes at the cost of an elevated temperature dependence of the capacitance value of +22%/−33% compared to the X7R MLCCs with ±15% for a temperature range of −55 °C-125 °C [2].

In practical applications, typically only the MLCC large-signal voltage swing U (or E_x) is known (cf. Fig. 1), while deriving the related charge variation Q (or D_x) is not trivial due to the non-linearity of the capacitance value [16]. Although the charge Q can be measured accurately by integrating the measured capacitor current (i.e., no Sawyer-Tower required), an estimation of $D_x\{E_x\}$ allows to calculate device losses without a device-specific measurement. The scatter points in Fig. 3(b) show the relative displacement field D_x (derived from the measured charge $Q\{U\}$) against the relative voltage excitation E_x. Generally, for a given MLCC series, a close matching of $D_x\{E_x\}$ curves can be observed, where some devices also deviate for larger relative excitation magnitudes.

For example, ① represents the only considered device of Kowles Syfer with $U_R = 200$ V, showing a different $D_x\{E_x\}$ curve than the other MLCCs of this series. Further, ② and ③ represent 1 μF MLCCs with $U_R = 500$ V and $U_R = 630$ V, respectively. The measurements reveal almost identical charge and loss behavior for these two devices, indicating a similar internal structure despite the different voltage ratings.

Both examples can be explained by a different safety margin to the maximum admissible electric field strength E_{max} selected for the devices, hence the underlying assumption in (6) of the device thickness linearly scaling with rated voltage does not always fully hold for real MLCCs. Despite this, a simple second order polynomial fit of $D_x\{E_x\}$ (represented by dashed lines in Fig. 3(b)) shows a maximum deviation of $\epsilon_{Dx} < 22\%$ (cf. Table I) and allows to calculate D_x with reasonable accuracy, where the modeling error ϵ_{Dx} is calculated as

$$\epsilon_{Dx} = \frac{D_{x,calc} - D_{x,meas}}{D_{x,meas}}. \tag{11}$$

Note, that typical X7R and X7T MLCCs show a nominal capacitance tolerance δ_C of either ±10% or ±20%, which according to (5) results due to geometrical (i.e., active area A or dielectric layer thickness t) or material tolerances (i.e., permittivity ε) occurring in the complex MLCCs manufacturing process [1] [2]. Accordingly, also the $Q\{U\}$ characterization of a device (which is required to employ the iGSE-C_Q (1)) is subject to a capacitance tolerance of up to ±20%. Furthermore, it should be noted that magnetic components are analogously also subject to relatively large geometrical

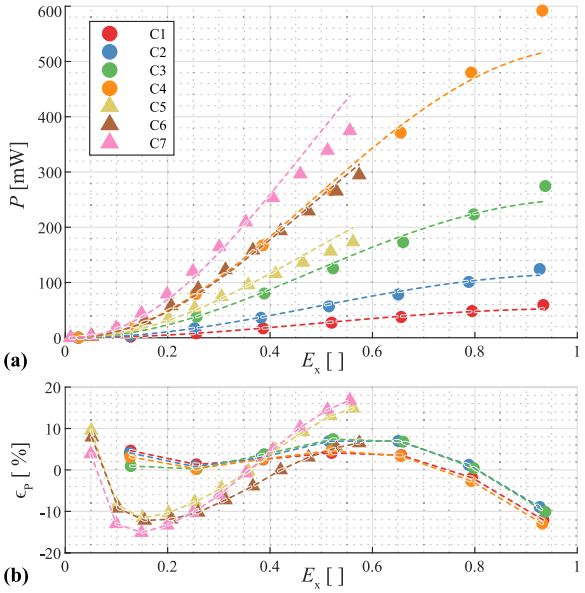

FIGURE 4. (a) Detailed measured losses (scatter points) and calculated losses with the iGSE-C_x (dashed lines) vs. relative electric field E_x for the TDK X7R MLCCs listed in Table II. (b) Resulting loss estimation error ϵ_P of the iGSE-C_x.

(core dimensions) and material tolerances, which are limiting the practical accuracy of flux density B_{pk} calculation and the Steinmetz loss modeling [23] [24].

Then, employing the iGSE-C_X parameters reported in Fig. 3(a), the derived $D_x\{E_x\}$ curves in Fig. 3(b), as well as the datasheet device parameters (i.e., U_R and C_0, cf. Appendix A), the large-signal excitation losses of an MLCC for a given voltage U can be calculated with (9). As an example, Fig. 4(a) details the measured (scatter points) and calculated losses (dashed lines) of the TDK X7T MLCC series (cf. Table II), while Fig. 4(b) shows the resulting modeling error ϵ_P (calculated analogously to (11), and displayed only for relative E-field excitation values $E_x > 3\%$), which is below 20%. The model deviation of the considered MLCC series is also summarized in Table I, where the maximum deviation of 51% results for the Knowles Syfer X7R series.

Hence, the iGSE-C_x shows lower precision compared to the iGSE-C_Q (with component-specific Steinmetz parameters) employed in [16]. However, performing an iGSE-C_Q characterization of each capacitor which is to be employed in a power converter is not practical (typically a large number of parallel devices is employed in a converter to realize large capacitance values), and therefore the previously discussed nominal capacitance tolerance δ_C of up to $\pm 20\%$ has anyway to be taken into account in the design process. With δ_C having a linear impact on the peak charge Q_{pk}, according to (1) an iGSE-C_Q model precision of $(1 \pm \delta_C)^\beta$ has to be considered, which translates for e.g., $\beta = 2.3$ to a range of $+52\%/-40\%$ and/or a similar precision as the iGSE-C_x.

While ①–③ discussed in this section (cf. Fig. 3(b)) illustrate how MLCC manufacturers could help improving the loss estimation and the accompanied relative displacement field $D_x\{E_x\}$ calculation by publishing the employed safety margin to the maximum admissible electric field strength E_{max} of each device, an upper bound for the precision of MLCC large-signal loss modeling is currently dictated by the nominal capacitance tolerance δ_C. There, a further improvement of the loss model could be enabled by more detailed information on geometrical device tolerances: According to (2) a tolerance in active area A impacts only the dielectric volume, while a tolerance in layer thickness t further impacts the resulting E-field and D-field, such that according to (3) a different influence on the device losses P results.

Hence, although in theory it is possible to model the losses of a complete MLCC series with the iGSE-C_x based upon Steinmetz parameters obtained by characterizing one single device, the discussion of the device tolerances clearly promotes considering several devices to enable more robust modeling results, where sufficient safety margin needs to be considered for practical designs. Here, it is important to also highlight, that the MLCC large-signal losses are not only relevant from a converter efficiency perspective, but also for the heat management to keep the MLCCs within the allowed operation temperature.

In summary, the results presented here show the feasibility of an approximate MLCC loss estimation during the converter design process based on datasheet values and a single set of iGSE-C_x parameters (which are valid for a complete MLCC series), where the model accuracy is acceptable, especially compared to the small-signal dissipation factor published by manufacturers which can be off by up to a factor of 10 (!) [16].

IV. APPLICATION EXAMPLE

In the following, the concept of the iGSE-C_x is employed to estimate large-signal MLCC losses in a practical example. The considered application is a three-phase variable speed drive inverter sinewave output filter, assuming a motor phase voltage of $230V_{rms}$ (line-to-neutral) and a stator frequency of 50 Hz (e.g., ABB 3GAA101520-ASJ, 3kW induction motor, $\approx$ 3000 rpm). The filter capacitors are arranged in star configuration, with the star point connected to the converter DC-link midpoint, such that the maximum capacitor voltage is given by the peak motor phase voltage of $325V_{pk}$. The required minimum capacitance value is 1.8 μF and the TDK X7T series is considered due to its superior loss performance compared to X7R dielectrics.

In order to limit the capacitance variation during one fundamental cycle, the C5750X7T2J474K250KE MLCC (cf. Table III) rated for $U_R = 630$ V and with nominal capacitance $C_0 = 470$ nF is selected. According to the datasheet [25], the small-signal capacitance value drops to 45% for a bias voltage of $325V_{pk}$, and considering the capacitance tolerance of $\delta_C = \pm 10\%$, the capacitance value of 1.8 μF can be realized by paralleling 10 devices.

To determine the worst-case losses, in a first step, the relative electric field E_x is calculated from the peak voltage excitation of $325V_{pk}$ and the device rated voltage of 630 V according to (8), where $E_x = 0.52$ results. With the second

order fit provided for $D_x\{E_x\}$ of the TDK X7T series in Table I (cf. Fig. 3(b)), the relative displacement field can be calculated as $D_x = 0.42$. This value is multiplied with the maximum capacitance tolerance (i.e., $1+\delta_C$), and conservatively $D_x = 0.46$ is used for the subsequent loss calculation.

Then, employing the iGSE-C_X in (9), the expected worst case large-signal losses per device result as 119mW. A loss measurement was conducted for the considered device and operating point with the MLCC test setup from Section III, and 98mW were recorded for this operating point, corresponding to a loss estimation error ϵ_P of 22%. Please note that with this test setup, the MLCC losses resulting due to the high-frequency operation of the motor drive inverter are not considered, however according to [16] the contribution of the high-frequency losses to the overall MLCC losses is small. Further, it is important to highlight that here the loss modeling error of 22% results mainly due to the considered worst case capacitance tolerance $\delta_C = +10\%$ in the loss calculation, which ensures safe operation of the employed MLCCs in this application (if neglecting the capacitance tolerance (i.e., $\delta_{C=0}$), the model error reduces to $\epsilon_P = -0.9\%$).

The calculated total capacitor losses of the sinewave filter are 3.6 W (corresponding to 0.1% of the nominal machine output power), while according to the datasheet [25], the calculated device losses translate into a device heating of 30 °C, which is tolerable.

V. CONCLUSION

Allowing for highly compact converter realizations, ferroelectric (non-linear) Class II Multilayer Ceramic Capacitors (MLCCs) are expected to further gain in importance. However, the Steinmetz modeling of large-signal excitation losses of MLCCs currently requires a large number of measurement points to characterize the parameters of the charge-based iGSE-C_Q model for a given device, which are not applicable to other devices of an MLCC series, i.e., not even for a manufacturer device series with similar geometries and the same dielectric material, but with different rated voltages and capacitance values.

In this paper, a new relative displacement field based Steinmetz model denoted as the iGSE-C_X is proposed and verified, which describes losses of a complete MLCC series. As the internal geometry of MLCCs is not disclosed by manufacturers, the iGSE-C_X only relies on datasheet information (i.e., the device rated voltage U_R and the nominal capacitance C_0). As an example, the large-signal excitation losses of the TDK X7R series can be calculated with a resulting error $< 20\%$. Although less precise than the iGSE-C_Q (with component-specific Steinmetz parameters), the material-specific iGSE-C_X allows to estimate large-signal losses of an MLCC series based on a single set of Steinmetz parameters, where the maximum resulting tolerance of the iGSE-C_X is still relatively small compared to a loss estimation based on the small-signal dissipation factor, which can be off by up to a factor of 10 (!) [16].

Furthermore, the power law relation between normalized losses and relative displacement field excitation D_x is verified for a range in D_x of two orders of magnitude (cf. Fig. 3(a)). With the assumed linear relationship of D_x and the displacement field D, the results hence also indicate the feasibility of a loss model based on the actual physical $D-E$ hysteresis curve, which is denoted as iGSE-C_D and would combine the advantages of the iGSE-C_Q (i.e precise loss calculation) and the iGSE-C_X (material-specific parameters). Accordingly, MLCC manufacturers could publish datasheets for their dielectric materials containing the iGSE-C_D parameters as well as a graph with $D\{E\}$ and eventually also several curves for DC-bias voltages or device temperatures. The MLCC device datasheet would then only need to contain a reference to the employed dielectric material, as well as the device total active area A and dielectric layer thickness t, allowing engineers to easily predict MLCC large-signal excitation losses during converter design, in a similar fashion as for magnetic materials.

ACKNOWLEDGMENT

The authors would like to thank Prof. Shmuel Ben-Yaakov for his highly valuable comments on the iGSE-C_Q loss modeling [16], finally motivating and inspiring the iGSE-C_X derivation. Furthermore, we would like to thank E. Kamata for developing the automated MLCC loss measurement setup and conducting a first set of MLCC loss measurements in the course of his DAS (Diploma of Advanced Studies) thesis at the Power Electronics Systems Laboratory (PES) of ETH Zurich.

APPENDIX A
COMPONENT DETAILS

TABLE II Considered TDK X7R MLCCs [21] (Cf. Fig. 4)

Part Number	Design.	U_R	C_0	k_Q	β
C3216X7R2E104K160AE	C1	250V	100nF	4.55e+07	2.29
C3225X7R2E224K200AE	C2	250V	220nF	1.60e+07	2.29
C4532X7R2E474K230KE	C3	250V	470nF	5.95e+06	2.29
C5750X7R2E105K230KE	C4	250V	1000nF	2.56e+06	2.30
C4532X7R2J104K230KE	C5	630V	100nF	3.04e+07	2.28
C5750X7R2J154K160KA	C6	630V	150nF	2.52e+07	2.31
C5750X7R2J224K230KE	C7	630V	220nF	9.82e+06	2.27

TABLE III Considered TDK X7T MLCCs [21]

Part Number	Design.	U_R	C_0	k_Q	β
C3216X7T2E224K160AE	-	250V	220nF	8.61e+05	2.11
C3225X7T2E334K200AE	-	250V	330nF	9.46e+05	2.17
C4532X7T2E105K250KE	-	250V	1000nF	3.17e+05	2.18
C5750X7T2E155K200KA	-	250V	1500nF	3.32e+05	2.23
C5750X7T2E225K250KE	-	250V	2200nF	1.76e+05	2.22
C3216X7T2W104K160AE	-	450V	100nF	3.05e+06	2.15
C3225X7T2W224K200AE	-	450V	220nF	1.63e+06	2.18
C4532X7T2W474K230KE	-	450V	470nF	7.76e+05	2.19
C5750X7T2W684K200KA	-	450V	680nF	5.28e+05	2.20
C5750X7T2W105K250KE	-	450V	1000nF	3.93e+05	2.20
C3225X7T2J104K160AE	-	630V	100nF	3.98e+06	2.18
C3225X7T2J154K200AE	-	630V	150nF	2.31e+06	2.17
C4532X7T2J224K200KE	-	630V	220nF	1.93e+06	2.20
C4532X7T2J304K250KA	-	630V	300nF	1.33e+06	2.20
C5750X7T2J474K250KE	-	630V	470nF	8.15e+05	2.20

TABLE IV Considered Knowles X7R MLCCs [22]

Part Number	Design.	U_R	C_0	k_Q	β
2220Y2000225KXTWS2	-	200V	2200nF	6.92e+05	2.26
1812Y2500105KXTWS2	-	250V	1000nF	1.81e+06	2.25
1812Y5000104KXT	-	500V	100nF	4.65e+07	2.29
1812Y5000224KJT	-	500V	220nF	2.07e+07	2.30
1812Y5000274KXT	-	500V	270nF	1.33e+07	2.31
2220Y5000334KXT	-	500V	330nF	8.87e+06	2.29
1812Y5000474KXTWS2	-	500V	470nF	4.01e+06	2.25
2220Y5000564KXT	-	500V	560nF	4.05e+06	2.28
2220Y5000105KXTWS2	-	500V	1000nF	1.68e+06	2.27
2220Y6300105KXTWS2	-	630V	1000nF	2.28e+06	2.30
1812Y1K00104KXT	-	1000V	100nF	2.99e+07	2.29
2220Y1K00104KXT	-	1000V	100nF	3.38e+07	2.28
1812Y1K00154KXTWS2	-	1000V	150nF	1.48e+07	2.26
2220Y1K00474KETWS2	-	1000V	470nF	5.39e+06	2.30
2220Y1K00474KETWS3	-	1000V	470nF	5.59e+06	2.30

REFERENCES

[1] M. Randall *et al.*, "Thin film MLCC," in *Proc. Symp. Passive Compon. (CARTS)*, Mar. 2007, Art. no. 403.

[2] M. J. Pan and C. Randall, "A brief introduction to ceramic capacitors," *IEEE Elect. Insul. Mag.*, vol. 26, no. 3, pp. 44–50, May/Jun. 2010.

[3] Y. Lei *et al.*, "A 2 kW single-phase seven-level flying capacitor multilevel inverter with an active energy buffer," *IEEE Trans. Power Electron.*, vol. 32, no. 11, pp. 8570–8581, Jan. 2017.

[4] D. Bortis, D. Neumayr, and J. W. Kolar, "$\eta - \rho$-Pareto optimization and comparative evaluation of inverter concepts considered for the google little box challenge," in *Proc. IEEE Workshop Control Model. Power Electron.*, Sep. 2016, pp. 1–5.

[5] F. Maislinger, H. Ertl, G. Stojcic, C. Lagler, and F. Holzner, "Design of a 100 kHz wide bandgap inverter for motor applications with active damped sine wave filter," *J. Eng.*, vol. 2019, no. 17, pp. 3766–3771, Apr. 2019.

[6] M. M. Swamy, J. Kang, and K. Shirabe, "Power loss, system efficiency, and leakage current comparison between si IGBT VFD and SiC FET VFD with various filtering options," *IEEE Trans. Ind. Appl.*, vol. 51, no. 5, pp. 3858–3866, Apr. 2015.

[7] G. Buja and G. Indri, "Improvement of pulse width modulation techniques," *Archiv Für Elektrotechnik*, vol. 57, no. 5, pp. 281–289, Sep. 1975.

[8] D. Neumayr, D. Bortis, J. W. Kolar, M. Koini, and J. Konrad, "Comprehensive large-signal performance analysis of ceramic capacitors for power pulsation buffers," in *Proc. IEEE Workshop Control Model. Power Electron.*, Jun. 2016, pp. 1–8.

[9] C. B. Barth, T. Foulkes, I. Moon, Y. Lei, S. Qin, and R. C. N. Pilawa-Podgurski, "Experimental evaluation of capacitors for power buffering in single-phase power converters," *IEEE Trans. Power Electron.*, vol. 34, no. 8, pp. 7887–7899, Oct. 2018.

[10] Z. Liao and R. C. N. Pilawa-Podgurski, "Power harmonic elimination technique for using non-linear ceramic capacitors under large voltage swings for single-phase active power decoupling," in *Proc. IEEE Workshop Control Model. Power Electron.*, Nov. 2020, pp. 1–7.

[11] A. Sheikholeslami and P. G. Gulak, "A survey of behavioral modeling of ferroelectric capacitors," *IEEE Trans. Ultrason., Ferroelectr., Freq. Control*, vol. 44, no. 4, pp. 917–924, Jul. 1997.

[12] I. Novak, K. B. Williams, R. Miller Jason, G. Blando, and N. Shannon, "DC and AC bias dependence of capacitors," in *Proc. DesignCon*, Jan. 2011, pp. 1–16.

[13] S. Ben-Yaakov, "Characterization of ferroelectric ceramic capacitors," in *Proc. 20th IEEE Eur. Conf. Power Electron. Appl.* (EPE-ECCE Europe), Sep. 2018, pp. 1–8.

[14] S. Ben-Yaakov, "Ceramic capacitors: Characterization and use as control elements," in *Proc. Tut. Power Convers. Intell. Motion Conf.*, May 2019.

[15] S. Coday, C. B. Barth, and R. C. N. Pilawa-Podgurski, "Characterization and modeling of ceramic capacitor losses under large signal operating conditions," in *Proc. IEEE Workshop Control Model. Power Electron.*, Jun. 2018, pp. 1–8. [Online]. Available: https://www.youtube.com/watch?v=yCK1hzgS_mU

[16] D. Menzi, D. Bortis, G. Zulauf, M. Heller, and J. W. Kolar, "Novel iGSE-C loss modeling of X7R ceramic capacitors," *IEEE Trans. Power Electron.*, vol. 35, no. 12, pp. 13 367–13383, Dec. 2020.

[17] L. E. Mosley and J. S. Schrader, "Hysteresis measurements of multilayer ceramic capacitors using a sawyer-tower circuit," in *Proc. Symp. Passive Compon.*, Jan. 2007, pp. 285–295.

[18] S. Ben-Yaakov, "Some observations on loss and hysteresis of ferroelectric-based ceramic capacitors," *IEEE Trans. Power Electron.*, vol. 33, no. 11, pp. 9127–9129, Nov. 2018.

[19] M. Randall, "A brief introduction to high voltage SMT capacitors," Venkel LTD., Tech. Rep. 035002 A4, 2007.

[20] J. Muhlethaler, J. Biela, J. W. Kolar, and A. Ecklebe, "Core losses under the DC bias condition based on Steinmetz parameters," *IEEE Trans. Power Electron.*, vol. 27, no. 2, pp. 953–963, Feb. 2012.

[21] "Multilayer ceramic chip capacitors," Datasheet, TDK Corporation", Feb. 2019. [Online]. Available: https://product.tdk.com

[22] " StackiCap high voltage high CV MLCC," AN0039, Knowles. [Online]. Available: https://www.knowlescapacitors.com

[23] F. Sixdenier, J. Morand, O. A. Salvado, and D. Bergogne, "Statistical study of nanocrystalline alloy cut cores from two different manufacturers," *IEEE Trans. Magn.*, vol. 50, no. 4, pp. 1–4, Apr. 2014.

[24] V. C. Valchev and A. Van Den Bossche, Inductors and Transformers for Power Electronics. Boca Raton, FL, USA: CRC press, 2018.

[25] " C5750X7T2J474K250KE," Datasheet, TDK Corporation, Mar. 2017. [Online]. Available: https://product.tdk.com

DAVID MENZI (Student Member, IEEE) received the B.Sc. degree in 2015 in electrical engineering and the M.Sc. degree in 2017 in information technology from the Swiss Federal Institute of Technology, ETH, Zürich, Switzerland, where he focused on power electronics, control theory, and high-voltage technology, and he also spent a semester as an Exchange Student with the Royal Institute of Technology, Stockholm, Sweden. Since February 2018, he has been working toward the Ph.D. degree with the Power Electronic Systems Laboratory, where he is focusing on ultra-compact three-phase inverter and rectifier systems with wide input–output voltage range. During his studies, he was with ABB Medium Voltage Drives, Turgi, Switzerland, as an intern and working student.

MORRIS HELLER (Student Member, IEEE) received the B.Sc. degree in 2014 in electric engineering from Hochschule Luzern/FHZ, Luzern, Switzerland, and the M.Sc. degree in 2018 in electrical engineering and information technology, with a focus on power electronic systems design and power semiconductors technology, from ETH Zürich, Zürich, Switzerland, where he is currently working toward the the Ph.D. degree with the Power Electronic Systems Laboratory, with a focus on three-phase rectifiers and multi port power converters.

JOHANN W. KOLAR (Fellow, IEEE) is currently a Full Professor and the Head of the Power Electronic Systems Laboratory with the Swiss Federal Institute of Technology ETH, Zürich, Switzerland. He has proposed numerous novel converter concepts including the Vienna Rectifier, the Sparse Matrix Converter, and the Swiss Rectifier, has spearheaded the development of x-million rpm motors, and has pioneered fully automated multi-objective power electronics design procedures. His research interests include ultra-compact/efficient WBG converter systems, ANN-based design procedures, solid-state transformers, ultra-high speed drives, and bearingless motors. He has supervised more than 75 Ph.D. students, authored or coauthored more than 900 journals and conference papers and four book chapters, and has filed more than 200 patents. From 2012 to 2016, he was a IEEE PELS Distinguished Lecturer. He was the recipient of more than 35 IEEE Transactions and Conference Prize Paper Awards, the 2014 IEEE Power Electronics Society R. David Middlebrook Achievement Award, the 2016 IEEE PEMC Council Award, the 2016 IEEE William E. Newell Power Electronics Award, and two ETH Zurich Golden Owl Awards for excellence in teaching. He was elected to the U.S. National Academy of Engineering as an International Member in 2021.